Octahedral tilts and electronic correlations in $La_{7/8}Sr_{1/8}MnO_3$

J. Geck,[1,2] P. Wochner,[2] S. Kiele,[1,3] P. Reutler,[1] A. Revcolevschi,[4] and B. Büchner[1]
[1]*Leibniz Institute for Solid State and Materials Research IFW Dresden, Helmholtzstrasse 20, 01069 Dresden, Germany*
[2]*Max-Planck-Institut für Metallforschung, Heisenberg Strasse 3, 70569 Stuttgart, Germany*
[3]*Hamburger Synchrotronstrahlungslabor HASYLAB at Deutsches Elektronen-Synchrotron DESY, Notkestrasse 85, 22603 Hamburg, Germany*
[4]*Laboratoire de Physico-Chimie de l'Etat Solide, Université de Paris-Sud, 91405 Orsay Cedex, France*
(Received 2 March 2006; revised manuscript received 16 July 2006; published 8 January 2007)

We present a resonant x-ray scattering study of the octahedral tilt order between 50 K and 310 K in $La_{7/8}Sr_{1/8}MnO_3$. At the La L_{II}-edge, the resonant (300) reflection probes cooperative tilts of the MnO_6 octahedra in this material, as verified by a model caclulation as well as a LDA+U study. The investigation of the octahedral tilts as a function of temperature and the comparison to the lattice parameters, the magnetization and the superlattice reflections related to charge and/or orbital order reveal an intimate coupling between electronic and tilt degrees of freedom in $La_{7/8}Sr_{1/8}MnO_3$.

DOI: 10.1103/PhysRevB.75.014405 PACS number(s): 71.30.+h, 61.10.Eq, 64.60.Cn, 71.27.+a

I. INTRODUCTION

The investigation of the electronic correlations in doped transition metal oxides is an active field of condensed matter research. In particular, the interplay between structural distortions and charge ordering phenomena has attracted a lot of attention. A prominent example for the coupling between structure and charges is the influence of the octahedral tilts on the stripe order in doped cuprates; i.e., the pinning of charge stripes by a potential due to tilts of the CuO_6 octahedra.[1,2] The static stripe order which develops in doped nickelates[3] might also be stabilized by a similar mechanism, namely by the cooperative tilting of the NiO_6 octahedra. Recently, it has been recognized that octahedral tilt order also plays an important role for the physics of doped manganites. In particular, there are indications that the tilting of the MnO_6 octahedra in $LaMnO_3$ couples to the orbital degree of freedom.[4,5]

In this paper we present a resonant x-ray scattering study of the octahedral tilt order in $La_{7/8}Sr_{1/8}MnO_3$ which shows several phase transitions as a function of temperature:[6,7] Upon cooling an orbital ordered state similar to that of $LaMnO_3$ develops at $T_{JT} \simeq 280$ K, where an antiferrodistortive ordering of Jahn-Teller distorted MnO_6 octahedra occurs.[8,9] Decreasing the temperature down to $T_C \simeq 180$ K leads to the onset of ferromagnetic order, yielding a change of the electrical resistivity from insulating to metal-like in agreement with the double exchange picture. Further cooling leads to a metal-insulator transition at $T_{CO} \simeq 155$ K, where a charge and orbital ordered ferromagnetic insulating (FMI) phase is established at low temperatures.[10–14] This FMI phase contradicts a bare double exchange model, and there is strong evidence that pronounced correlations between magnetism, charges, structure, and orbital degrees of freedom stabilize an orbital polaron lattice below T_{CO}.[15]

These results together with the aforementioned connection between the orbital order and the octahedral tilts found in $LaMnO_3$ raise the question whether octahedral tilts are important for the stabilization of the various phases in $La_{7/8}Sr_{1/8}MnO_3$ as well. In order to elucidate the role of the tilt ordering in $La_{7/8}Sr_{1/8}MnO_3$ we have performed resonant x-ray scattering (RXS) at the La L_{II}-edge which has been shown to be highly sensitive to changes in the octahedral tilt order.[4,16]

II. EXPERIMENTAL TECHNIQUE

By tuning the x-ray energy to the La L_{II}-edge the scattering process involves $2p \rightarrow 5d$ transitions in the La subbands; i.e., the creation of virtual photoelectrons in an intermediate $5d$ state. This results in a highly increased sensitivity to changes of the octahedral tilt order, as can be understood in terms of a model calculation based on a purely ionic picture: Adopting the dipole-dipole approximation the relevant term of the atomic form factor f near the La L_{II}-edge can be described by a second rank tensor $\hat{f}$ with respect to the beam polarization, which is given by[17,18]

$$\hat{f}^{(\alpha,\beta)} = \frac{1}{m}\sum_j \frac{\langle 2p|p_\alpha|5d_j\rangle\langle 5d_j|p_\beta|2p\rangle}{E(5d_j) - E(2p) - \hbar\omega - i\Gamma/2}.$$

Here, $|2p\rangle$ and $|5d_j\rangle$ denote the initial $2p$ state and the $5d$ intermediate states, respectively. $E(2p)$ and $E(5d_j)$ are the corresponding energies, m is the (reduced) electron mass, $p_{\alpha,\beta}$ $(\alpha,\beta=1,2,3)$ represents the components of the momentum operator, and $\Gamma \sim 1$ eV is the lifetime broadening width of the $2p$ core hole.

Since the asymmetric unit of the $LaMnO_3$ structure contains only a single lanthanum site, the structure factor tensor used for the kinematic calculation of the diffracted intensities reads (temperature effects are neglected)[19]

$$\hat{F}(\mathbf{Q}) = \sum_g \hat{f}_g e^{i\mathbf{Q}\cdot\mathbf{r}_g}.$$

In the above equation the sum runs over the symmetry operations g of the space group, $\hat{f}_g = R_g \hat{f} R_g^t$ is the scattering factor tensor transformed by the rotational part R_g of g, $\mathbf{r}_g$ is the position vector of the corresponding symmetry related lattice site and $\mathbf{Q}$ stands for the scattering vector. Note that

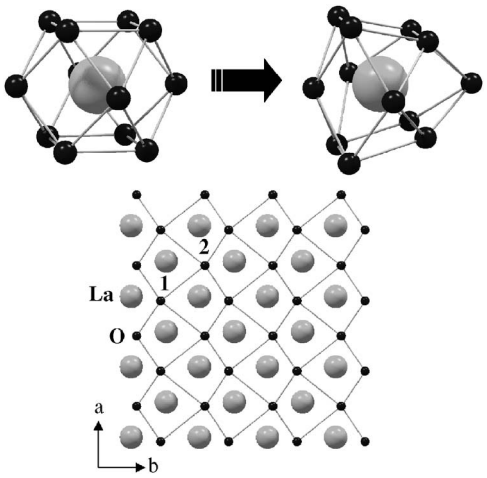

FIG. 1. Top: Deformation of the oxygen cage around a lanthanum ion in the orbital ordered phase of $LaMnO_3$ (the edges of the cage do not represent chemical bonds). Bottom: The tilt order in the orbital ordered phase creates lanthanum sites with differently distorted local environments in the orthorhombic *ab* plane (sublattices 1 and 2).

due to the above transformation of $\hat{f}$ the form factor tensor of the lattice sites 1 and 2 in Fig. 1 is different. This corresponds to the fact that the local distortions around sites 1 and 2 are different. For a *Pbnm* symmetry, which we refer to throughout this paper, the intensities of the forbidden (300) reflection in the $\sigma\pi$ and the $\sigma\sigma$ channel are[20]

$$I_{\sigma\pi} \propto (f_{12} \cos\vartheta \cos\Phi)^2,$$

$$I_{\sigma\sigma} = 0,$$

where ϑ is the Bragg angle and Φ is the azimuthal angle, which describes the rotation of the sample around the scattering vector.[9] In the ionic picture the matrix element f_{12} can then be calculated using the Wigner-Eckhart theorem, in order to get an idea of its dependence on octahedral tilts and distortions. For a $2p_{1/2}$ initial state and the $5d$ intermediate states of t_{2g} and e_g symmetry it follows (the same result holds for a $2p_{3/2}$ initial state):

$$f_{12} = \frac{|M|^2}{E(5d_{yz}) - E(2p) - \hbar\omega - i\Gamma/2} - \frac{|M|^2}{E(5d_{xz}) - E(2p) - \hbar\omega - i\Gamma/2} \propto |M|^2 \Delta \times \mathcal{L}_\Delta(\hbar\omega).$$

Here, $|M|^2$=const has the unit of an energy, $\Delta = E(5d_{xz}) - E(5d_{yz})$, and $\mathcal{L}_\Delta(\hbar\omega)$ is a Lorentzian centered at Δ. Since the t_{2g} symmetric $5d_{xz}$ and $5d_{yz}$ orbitals are degenerate in a cubic crystal field, the intensity of the (300) vanishes in this case ($\Delta=0$). But since octahedral tilts and distortions lower the symmetry of the local environment, this orbital degeneracy is lifted ($\Delta \neq 0$). In this case $I_{\sigma\pi}$ does not vanish and the (300) reflection is observed at the La L_{II}-edge. As a result, the ionic model yields the occurrence of the resonant (300) reflection at the La L_{II}-edge for nonvanishing octahedral tilts and/or distortions with three important main characteristics, namely (i) pure $\sigma\pi$ scattering, (ii) a $\sin^2$ azimuthal dependence, and (iii) a resonant increase of the intensity at the La edges. This is in agreement with an experimental RXS study at the La L_{II}-edge on $LaMnO_3$.[4] But as will be described in the following, these features of the resonant scattering at the La L_{II}-edge are also observed for hole doped $La_{7/8}Sr_{1/8}MnO_3$, whose average structure can be described in terms of a *Pbnm* symmetry although there are slight deviations from this symmetry below T_{JT}.[21–24]

However, the ionic picture has also its limitations. More specifically, the dependence of f_{12} on the values of the tilt angles and the size of the distortions cannot be calculated accurately. This is because band structure effects, which are relevant for the spatially extended La:5d intermediate states, are not taken into account in this description. Therefore, the ionic localized valence charge model should only be used as a guide, whereas a rigorous discussion should always refer to the full band-structure calculation. In a previous paper, the effect of structural distortions on the (300) reflection at the La edges has been calculated by means of LDA+U, which provides an appropriate description for the effects of the band structure mentioned above.[16] Besides the octahedral tilts also distortions of the octahedra have been investigated. But the LDA+U calculations show that the intensity of the (300) reflection at the La L_{II}-edge is mainly given by octahedral tilts, whereas the contribution due to distortions of the octahedra has been found to be negligible. This theoretical result is also verified experimentally by a RXS study on $LaMnO_3$.[4] The results described above show that the interpretation of the (300) intensity in the $\sigma\pi$ channel at the La L_{II}-edge in terms of octahedral tilts is well justified.

The RXS experiment has been performed using a vertical scattering geometry at the wiggler beamline *W*1 at HASYLAB. This beamline is equipped with a Si(111) double monochromator which provides an energy resolution of about 2 eV at the La L_{II}-edge. The sample was mounted on the cold finger of a closed cycle cryostat which was itself mounted on a standard Eulerian cradle. The incident slits have been chosen in order to give a polarization $P = I^\sigma/(I^\sigma + I^\pi) = 0.93$ of the incident beam, where σ and π refer to polarization directions perpendicular and parallel to the scattering plane, respectively. For the polarization analysis at the La L_{II}-edge the (004) reflection of graphite with a scattering angle of $2\Theta \simeq 77.61°$ has been used, leading to a cross talk between $\sigma\sigma$ and $\sigma\pi$ channels of 6% as determined from the (400) Bragg reflection. The $La_{7/8}Sr_{1/8}MnO_3$ single crystals have been grown using the traveling floating zone method[25] and for the RXS experiment a sample with a polished (100) surface has been prepared (surface roughness $\simeq 5$ μm).

III. RESULTS

A. Energy and azimuthal dependence

Figure 2 displays the energy dependence of the (300) reflection around the La L_{II}-edge at 50 K in the FMI phase. The energy dependence displays a sharp (full width at half-maximum $\simeq 5$ eV) but asymmetric peak at 5897 eV and a broad increase of the resonant intensity around 5926 eV. Above 5940 eV and below 5890 eV the intensity at the (300)

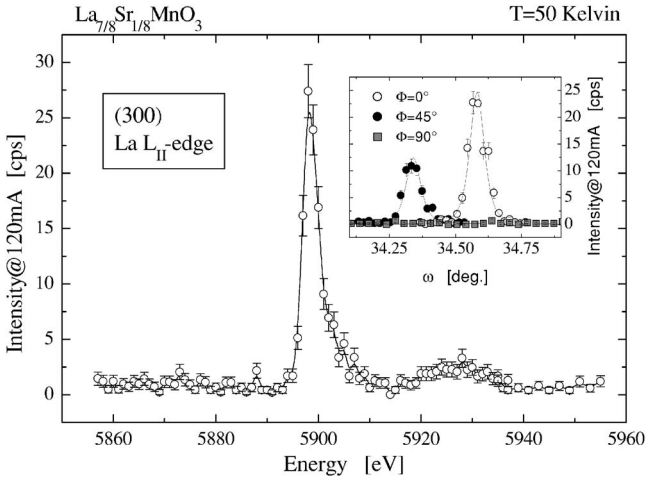

FIG. 2. Energy dependence of the (300) reflection around the La L_{II}-edge in the FMI phase at 50 K. The azimuthal dependence of a rocking scan at the same temperature and at 5987 eV is shown in the inset. These measurements have been performed without analyzer.

position vanishes within the investigated energy window. The observed features of the energy dependence shown in Fig. 2 resemble the calculated energy dependence at the La L_{II}-edge obtained by the LDA+U calculations mentioned above. In the inset of Fig. 2 the pronounced azimuthal dependence of a rocking scan through the (300) reflection at 5897 eV can clearly be observed. Referring to the inset, the case $\Phi=0°$ corresponds to a polarization of the incident beam parallel to the a,b direction, whereas this polarization is perpendicular to the ab plane for $\Phi=90°$. Obviously, the intensity is continuously reduced to zero by increasing Φ from 0° to 90°, excluding multiple scattering as the origin for the intensity at the (300) position. The polarization analysis performed using the (004) reflection of graphite reveals that, within the experimental errors, the resonant scattering at the La L_{II}-edge occurs only in the $\sigma\pi$ channel.

In Fig. 3, the energy dependences of the (300) reflection taken at 50 K, 157 K, 200 K, and 285 K are compared. It can be seen that the shape of the resonance curve is not affected by increasing the temperature; i.e., the overall line shape of the energy dependence is the same in the FMI phase ($T<T_{CO}\simeq 155$ K), the cooperative Jahn-Teller distorted phase ($T_{CO}<T<T_{JT}\simeq 280$ K) and above T_{JT}. In addition, only $\sigma\pi$ scattering could be observed in the different phases. The features of the resonant scattering correspond exactly to what is expected for *Pbnm* symmetry (cf. Sec. II), although the lattice symmetry is reduced at the phase transitions from orthorhombic to monoclinic to triclinic upon cooling.[24,26] This indicates that the tilt pattern, which describes in which way the octahedra tilt with respect to each other, always corresponds to the tilt pattern that is realized for *Pbnm* symmetry. In other words, the data indicate that the tilt pattern of $La_{7/8}Sr_{1/8}MnO_3$ is unchanged across the phase transition at T_{CO} and T_{JT}, in agreement with earlier conclusions.[24]

However, it becomes apparent that the intensity of the (300) reflection is strongly temperature dependent as will be discussed in the following.

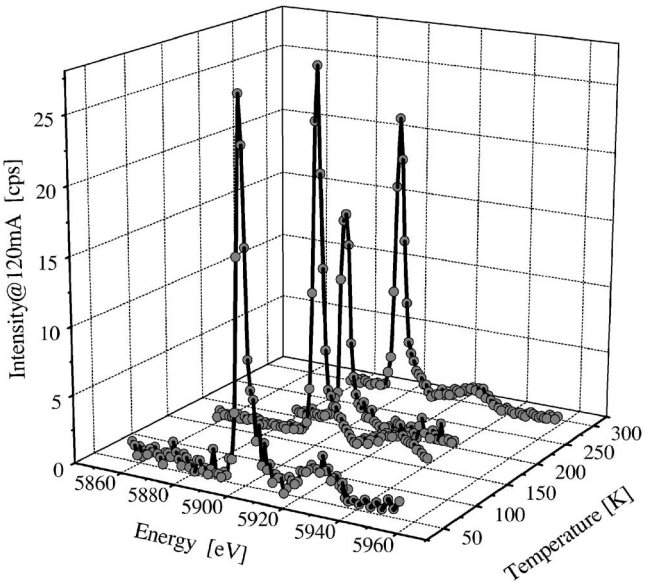

FIG. 3. Comparison between the energy dependences of the (300) reflection taken at 50 K, 157 K, 200 K, and 285 K. The shape of the resonance curve is unchanged with increasing temperature whereas the intensity is temperature dependent.

B. Temperature dependence

Figure 4(a) deals with a comparison between the temperature dependences of the a,b axis, the integrated intensity of the (4,0,0.5) and the (300) reflection measured at the Mn K-edge, as well as the (300) reflection measured at the La L_{II}-edge. In addition to this, the temperature dependence of $|\gamma|^{-1}$, where $\gamma=2(a-b)/(a+b)$ is the orthorhombic strain in the ab plane, and the macroscopic magnetization is given in Fig. 4(b). (4,0,0.5) is a superstructure reflection which has been discussed in relation to charge order within the FMI phase.[11,27,28]

Upon cooling a cooperative Jahn-Teller distorted and antiferro-orbital ordered phase develops at T_{JT}, which is schematically shown in Fig. 4(c).[21] The corresponding structural phase transition is clearly reflected by the anomalies of the lattice parameters a and b, which cross at this temperature. At the Mn K-edge, RXS is sensitive to octahedral distortions[16,26] and, therefore, the strong increase of the (300) reflection at the Mn K-edge signals the onset of cooperative octahedral distortions at T_{JT}. In contrast to the sensitivity to distortions at the Mn K-edge, the (300) reflection becomes sensitive to changes of the cooperative octahedral tilts for photon energies at the La L_{II}-edge. This means that the increase of the (300) reflection at the La L_{II}-edge upon cooling reveals changes of the cooperative octahedral tilts at T_{JT}. According to the discussion in the preceding section, these changes most likely affect merely the tilt angles but not the tilt pattern.

With further decreasing temperature, the ab splitting and the cooperative Jahn-Teller distortions grow as can be seen in the two upper panels of Fig. 4(a), until both reach a maximum at the ferromagnetic ordering temperature T_C. At the same time, the concomitant reduction of the (300) intensity at the La L_{II}-edge indicates a coupling between the octahedral tilts and distortions.

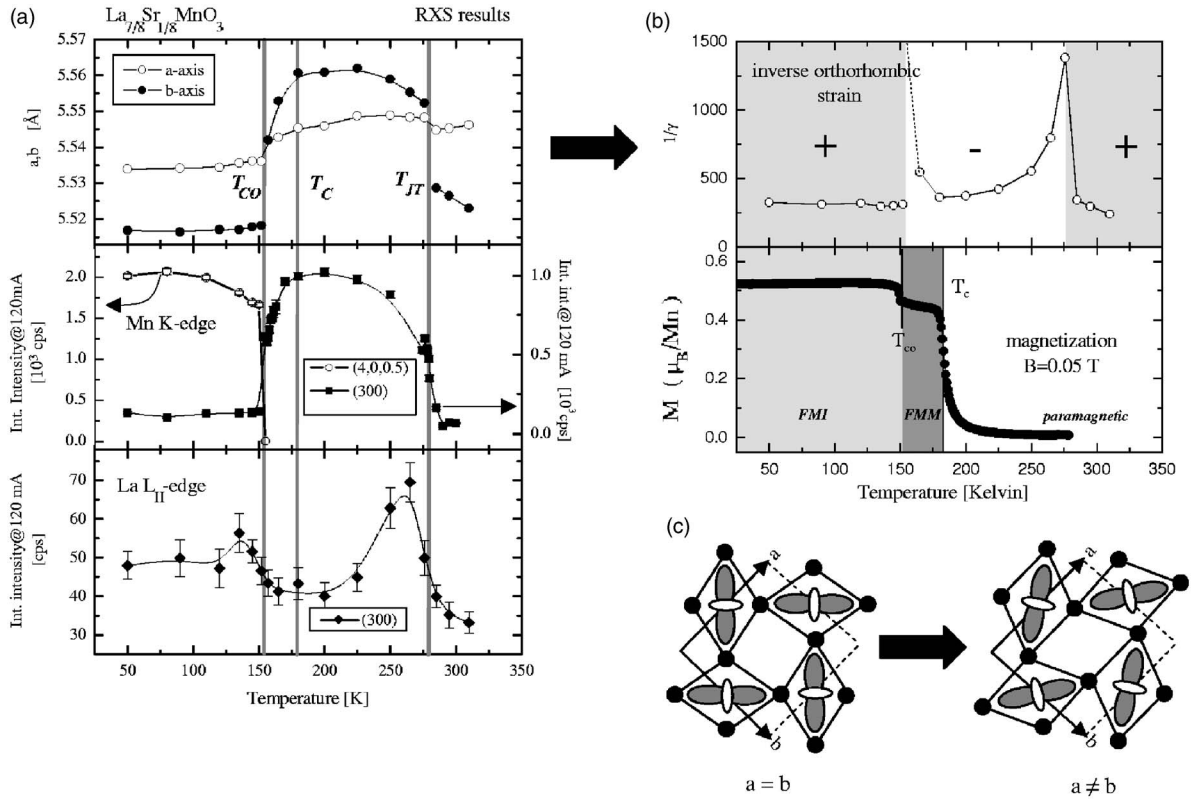

FIG. 4. (a) Comparison of the temperature dependences of the lattice parameters (top), the integrated intensity of the (4,0,0.5) as well as the (300) reflection at the Mn *K*-edge (middle), and the integrated intensity of the (300) reflection at the La L_{II}-edge (bottom). The measurements have been performed with increasing temperature. (b) Temperature dependence of $|\gamma|^{-1}$, where $\gamma=2(a-b)/(a+b)$ is the orthorhombic strain in the *ab* plane (top), and the macroscopic magnetization (bottom). The +/− signs in the top panel indicate the sign of γ. (c) Illustration of the connection between the a,b splitting, the octahedral distortions, and the octahedral tilts in the cooperative Jahn-Teller distorted phase. Without tilts there is no a,b splitting, while a finite tilt around the *c* axis (perpendicular to the paper plane) results in $a \neq b$. The gray and white lobes represent the occupied e_g states.

The magnetization increase at $T_C \simeq 180$ K shown in Fig. 4(b) marks the onset of ferromagnetic spin order. In agreement with the double exchange (DE) mechanism, the onset of ferromagnetic order below T_C is connected to an enhanced charge carrier mobility, i.e., metal-like behavior.[6] Therefore, this phase will be referred to as ferromagnetic metallic phase (FMM) in the following. As can be observed in Fig. 4(a), the *ab* splitting as well as the intensity of the (300) reflection at the Mn *K*-edge is reduced drastically with increasing ferromagnetic order. The temperature dependence of the (300) at the Mn *K*-edge implies a suppression of the cooperative Jahn-Teller distortions in the FMM phase upon cooling. However unlike the behavior observed around T_{JT}, the suppression of the octahedral distortions is not accompanied by pronounced changes of the (300) intensity at the La L_{II}-edge below T_C, indicating that the octahedral tilts hardly change in the FMM phase.

Finally, the *a* and *b* axes cross again, the (300) reflection at the Mn *K*-edge collapses, and new superstructure reflections like the (4,0,0.5) reflection shown in Fig. 4(a) (middle) occur at T_{CO} upon cooling. In a recent paper we showed that the metal-insulator transition at T_{CO} is connected to a reordering in the orbital sector, leading to the occurrence of new superlattice reflections.[26] More specifically, we revealed that upon cooling the antiferro-orbital order vanishes at T_{CO} and an orbital polaron lattice is formed.[15] This orbital polaron lattice leads to enhanced ferromagnetic interactions in agreement with the magnetization jump at T_{CO} that can be observed in Fig. 4(b). The moderate increase of the (300) reflection at the La L_{II}-edge shows that the orbital reordering at the metal-insulator transition is also connected to changes of the cooperative octahedral tilting, most likely the tilt angles.

At last, we note another interesting experimental observation, which concerns the continuous behavior of the (300) reflection at the La L_{II}-edge across the first order phase transitions at T_{JT} and T_{CO}. For the transition into the cooperative Jahn-Teller distorted phase a similar observation has been reported for $LaMnO_3$.[4,29]

IV. DISCUSSION

The data shown in Fig. 4 demonstrate the coupling of structural and electronic degrees of freedom in $La_{7/8}Sr_{1/8}MnO_3$. In the following the coupling between the octahedral tilts to other degrees of freedom will be discussed in more detail.

First we note, that the *ab* splitting is determined by two effects in general, namely the octahedral tilts and distortions. However, in the case of a $GdFeO_3$ type tilt order and mod-

erate variations of the tilt angles, the *ab* splitting can be approximated as

$$a-b=(a-b)_0+2^{3/2}\delta d(\eta_0+\delta\eta)+O(\delta d\,\delta\alpha)$$
$$\simeq (a-b)_0+2^{3/2}\delta d\,\eta_0$$

[$(a-b)_0$, *ab* splitting just above T_{JT}; δd, difference between the short and the long Mn-O bond parallel to the *ab* plane; $\delta\alpha$, temperature dependent variation of tilt angle around the *a* or *b* axis; η_0, the tilt angle around the *c* axis above T_{JT}; $\delta\eta$, temperature dependent variation of η_0]. In the final expression terms proportional to $(\delta\eta\delta d),(\delta\alpha\delta d)\ll 1$ have been neglected. Typical values for $T_{CO}<T<T_{JT}$ are about $\eta_0\simeq 15°$ and $\delta d\simeq 0.02$ Å.

The term proportional to $\eta_0\delta d$ in the above equation expresses the fact that to leading order $\delta d\neq 0$ does not lead to any increase of $(a-b)$ as long as $\eta_0=0$ (cf. Fig. 4). This term further implies that the temperature dependent changes of $(a-b)$ are mainly given by the distortions of the octahedra, as verified by the experimental data shown in the two upper panels of Fig. 4(a). In this figure it can be observed that the *ab* splitting is directly related to the octahedral distortions detected by the (300) reflection at the Mn *K*-edge.

Above T_{JT}, the octahedra are undistorted on average and the *ab* splitting can be attributed to the tilting of the octahedra. However, below T_{JT} the onset of octahedral distortions ($\delta d\neq 0$) changes the *ab* splitting according to the above equation. The increasing δd leads to a sign change of the orthorhombic strain with increasing δd [cf. top panel of Fig. 4(b)] and causes a small *ab* splitting close to T_{JT}. With further decreasing temperature, δd increases yielding a large negative orthorhombic strain. Finally, below T_C the octahedral distortions are reduced and eventually vanish at T_{CO}, where the sign of the orthorhombic strain changes back to positive.

Focusing on the temperature regime above T_C, it can be observed that the intensity of the (300) reflection at the La L_{II}-edge as a function of temperature behaves similar to $|\gamma|^{-1}$, where γ is the orthorhombic strain in the *ab* plane defined above. In other words, above T_C an increased orthorhombic strain is related to a decrease of the (300) intensity at the La L_{II}-edge. This shows that *in the paramagnetic phase the variations of the octahedral tilts above* T_C *are directly coupled to changes of the lattice strain*; i.e., the elastic energy of the lattice. It can therefore be concluded that in the paramagnetic phase the antiferro-orbital ordering and the octahedral tilts are coupled mainly via the elastic energy of the lattice.

However, this situation changes below the ferromagnetic transition temperature T_C. Although the *ab* splitting is strongly reduced in the FMM phase upon cooling ($|\gamma|^{-1}$ diverges), the (300) intensity at the La L_{II}-edge hardly changes, revealing that there are almost no changes of the octahedral tilts. This implies that below T_C the tilts are no longer only influenced by changes of the elastic energy. Otherwise, in analogy to the Jahn-Teller transition at T_{JT}, we would expect a strong increase of the (300) intensity at the La L_{II}-edge due to the decrease of the orthorhombic strain.

In fact, in the FM ordered phases the DE mechanism becomes important, which favors larger Mn-O-Mn bond angles, i.e., smaller tilts. Hence, the behavior of the (300) intensity at the La L_{II}-edge below T_C implies that *in the FMM phase the octahedral tilts are also strongly coupled to the double exchange*, a purely electronic mechanism.

The stabilization of a particular octahedral tilt pattern in $A_{1-x}B_xMnO_3$ is mainly attributed to the coordination of the A/B sites.[30] More specifically, different tilt pattern lead to different coordinations of these sites and, thereby, yield different energies. However, the experimental data presented here reveal that the octahedral tilts in $La_{7/8}Sr_{1/8}MnO_3$ are also strongly affected by the electronic properties related to the correlated Mn:3*d* and O:2*p* electrons. One coupling mechanism between the correlated electron system and the octahedral tilts is given by the transfer integral *t*, which depends on the Mn-O-Mn bond angles and, therefore, on the octahedral tilts. Since the physics of doped manganites are governed by various competing interactions, the coupling of the electronic degrees of freedom and the octahedral tilting observed here is expected to have a significant impact on the stability of the various ordered phases.

V. CONCLUSION

The energy, azimuthal, and temperature dependence of the symmetry forbidden (300) reflection at the La L_{II}-edge has been investigated. As discussed in Sec. II, the intensity changes of the (300) reflection at this energy are dominated by changes of the octahedral tilt order and are almost insensitive to pure octahedral distortions.

The presented experimental results show that the various ordering phenomena observed in $La_{7/8}Sr_{1/8}MnO_3$ couple to the cooperative octahedral tilts. This conclusion is further supported by the effects of chemical pressure on $La_{7/8}Sr_{1/8}MnO_3$: Upon substituting La by smaller Pr in $(La_{1-y}Pr_y)_{7/8}Sr_{1/8}MnO_3$, the mean radius of the corresponding lattice site (the so-called *A* site) can be reduced in a systematic way, resulting in an increase of the octahedral tilts.[30] Upon increasing the Pr concentration *y* the transition temperature T_{CO} is considerably reduced, while T_{JT} is strongly increased.[14] However, it must be noted that substitution of La by Pr also increases the variance of the *A*-site cation size, which could influence the transition temperatures T_{CO} and T_{JT} as well.[31] But experiments as a function of external pressure, i.e., at constant variance of the *A*-site radius, reveal changes of T_{CO} and T_{JT} that are in line with the effects observed upon Pr doping.[32–34] These studies therefore strongly support the main finding of this study, namely the intimate relation of the octahedral tilting and the various ordering phenomena in $La_{7/8}Sr_{1/8}MnO_3$.

Also at other doping levels there are clear indications for the relevance of octahedral tilts for the physical properties of doped manganites. For instance, the mean ionic radii of the *A* site have also a strong influence on the stability of the charge and orbital ordered CE phase in half-doped manganites.[35] This points to the important role of the octahedral tilting for the physics of doped manganites in general.

The tilt order is not only of importance in the case of manganites, as already mentioned in the Introduction. This order parameter also plays a crucial role for the physics of other transition metal oxides like nickelates and cuprates. Also in these cases the RXS technique is perfectly suited to study octahedral tilt order and its coupling to other degrees of freedom.

ACKNOWLEDGMENTS

The authors would like to thank M. v. Zimmermann for the careful reading of our paper and many useful discussions. The authors are very grateful to H. Dosch for his support. This work was supported by the Deutsche Forschungsgemeinschaft.

[1] J. M. Tranquada, B. J. Sternlieb, J. D. Axe, Y. Nakamura, and S. Uchida, Nature (London) **375**, 561 (1995).
[2] B. Büchner, M. Breuer, A. Freimuth, and A. P. Kampf, Phys. Rev. Lett. **73**, 1841 (1994).
[3] J. M. Tranquada, D. J. Buttrey, V. Sachan, and J. E. Lorenzo, Phys. Rev. Lett. **73**, 1003 (1994).
[4] M. Zimmermann, C. Nelson, Y.-J. Kim, J. Hill, D. Gibbs, H. Nakao, Y. Wakabayashi, Y. Murakami, Y. Tokura, Y. Tomioka *et al.*, Phys. Rev. B **64**, 195133 (2001).
[5] T. Mizokawa, D. I. Khomskii, and G. A. Sawatzky, Phys. Rev. B **60**, 7309 (1999).
[6] S. Uhlenbruck, R. Teipen, R. Klingeler, B. Büchner, O. Friedt, M. Hücker, H. Kierspel, T. Niemöller, L. Pinsard, A. Revcolevschi *et al.*, Phys. Rev. Lett. **82**, 185 (1999).
[7] R. Klingeler, J. Geck, R. Gross, L. Pinsard-Gaudart, A. Revcolevschi, S. Uhlenbruck, and B. Büchner, Phys. Rev. B **65**, 174404 (2002).
[8] H. Kawano, R. Kajimoto, M. Kubota, and H. Yoshizawa, Phys. Rev. B **53**, R14709 (1996).
[9] Y. Murakami, J. P. Hill, D. Gibbs, M. Blume, I. Koyama, M. Tanaka, H. Kawata, T. Arima, Y. Tokura, K. Hirota *et al.*, Phys. Rev. Lett. **81**, 582 (1998).
[10] Y. Endoh, K. Hirota, S. Ishihara, S. Okamoto, Y. Murakami, A. Nishizawa, T. Fukuda, H. Kimura, H. Nojiri, K. Kaneko *et al.*, Phys. Rev. Lett. **82**, 4328 (1999).
[11] Y. Yamada, J. Suzuki, K. Oikawa, S. Katano, and J. A. Fernandez-Baca, Phys. Rev. B **62**, 11600 (2000).
[12] M. Korotin, T. Fujiwara, and V. Anisimov, Phys. Rev. B **62**, 5696 (2000).
[13] T. Mizokawa, D. I. Khomskii, and G. A. Sawatzky, Phys. Rev. B **61**, R3776 (2000).
[14] J. Geck, P. Wochner, S. Kiele, R. Klingeler, P. Reutler, A. Revcolevschi, M. v. Zimmermann, and B. Büchner, New J. Phys. **6**, 152 (2004a).
[15] J. Geck, P. Wochner, S. Kiele, R. Klingeler, P. Reutler, A. Revcolevschi, and B. Büchner, Phys. Rev. Lett. **95**, 236401 (2005).
[16] P. Benedetti, J. van den Brink, E. Pavarini, A. Vigliante, and P. Wochner, Phys. Rev. B **63**, 060408(R) (2001).
[17] S. Ishihara and S. Maekawa, Phys. Rev. B **62**, 5690 (2000).
[18] M. Takahashi, J. Igarashi, and P. Fulde, J. Phys. Soc. Jpn. **68**, 2530 (1999).
[19] A. Kirfel, *Resonant Anomalous X-ray Scattering* (North-Holland, Amsterdam, 1994), Chap. II, p. 231.
[20] W. Morgenroth, *Resonant Anomalous X-ray Scattering* (North-Holland, Amsterdam, 1994), Chap. II, p. 257.
[21] L. Pinsard, J. Rodriguez-Cavajal, and A. Revcolevschi, J. Alloys Compd. **262-263**, 152 (1997).
[22] J. F. Mitchell, D. N. Argyriou, C. D. Potter, D. G. Hinks, J. D. Jorgensen, and S. D. Bader, Phys. Rev. B **54**, 6172 (1996).
[23] B. Dabrowski, X. Xiong, Z. Bukowski, R. Dybzinski, P. W. Klamut, J. E. Siewenie, O. Chmaissem, J. Shaffer, C. W. Kimball, J. D. Jorgensen *et al.*, Phys. Rev. B **60**, 10186 (1999).
[24] D. E. Cox, T. Iglesias, E. Moshopoulou, K. Hirota, K. Takahashi, and Y. Endoh, Phys. Rev. B **64**, 024431 (2001).
[25] P. Reutler, O. Friedt, B. Büchner, M. Braden, and A. Revcolevschi, J. Cryst. Growth **249**, 222 (2003).
[26] J. Geck, P. Wochner, D. Bruns, B. Büchner, U. Gebhardt, S. Kiele, P. Reutler, and A. Revcolevschi, Phys. Rev. B **69**, 104413 (2004).
[27] Y. Yamada, O. Hino, S. Nohdo, R. Kanao, T. Inami, and S. Katano, Phys. Rev. Lett. **77**, 904 (1996).
[28] T. Niemoeller, M. v. Zimmermann, S. Uhlenbruck, O. Friedt, B. Büchner, T. Frello, N. Andersen, P. Berthet, L. Pinsard, A. D. Léon-Guevara *et al.*, Eur. Phys. J. B **8**, 5 (1999).
[29] J. Rodriguez-Carvajal, M. Hennion, F. Moussa, A. H. Moudden, L. Pinsard, and A. Revcolevschi, Phys. Rev. B **57**, R3189 (1998).
[30] P. M. Woodward, Acta Crystallogr., Sect. B: Struct. Sci. **53**, 32 (1997).
[31] J. Attfield, Chem. Mater. **10**, 3239 (1998).
[32] Y. Moritomo, A. Asamitsu, and Y. Tokura, Phys. Rev. B **56**, 12190 (1997).
[33] M. Itoh, K. Nishi, J. D. Yu, and Y. Inaguma, Phys. Rev. B **55**, 14408 (1997).
[34] R. Klingeler, J. Geck, S. Arumugam, N. Tristan, B. Büchner, and A. Revcolevschi, Phys. Rev. B (to be published).
[35] Y. Tokura and N. Nagaosa, Science **288**, 462 (2000).